Estimation of magnetopause motion from low-energy neutral atom emission

K. Hosokawa,[1] S. Taguchi,[1] S. Suzuki,[1] M. R. Collier,[2] T. E. Moore,[2] and M. F. Thomsen[3]

Received 26 February 2008; accepted 23 July 2008; published 11 October 2008.

[1] A new method for deriving the position of the dayside equatorial magnetopause directly from the measured intensity of energetic neutral atom (ENA) emissions is presented. This approach makes it possible to track the position of the magnetopause using data observed by the low-energy neutral atom (LENA) imager on board the Imager for Magnetopause-to-Aurora Global Exploration (IMAGE) spacecraft. The model is applied to data recorded during a period of high solar wind dynamic pressure on 13 April 2001. In this interval, significant ENA flux was observed originating from the dayside low-latitude magnetosheath. This ENA flux is primarily the result of enhanced charge exchange between the increased solar wind plasma and exospheric hydrogen neutrals. The temporal variation in the estimated magnetopause position is compared with in situ measurements of magnetopause crossings by the LANL-01A spacecraft in geosynchronous orbit and the results of a recent empirical magnetopause model. It is demonstrated that the subsolar distance of the magnetopause was successfully tracked for a period of more than 1 h. In this particular case example, the dayside magnetopause is closer to the Earth and fluctuates on a shorter timescale than predicted by the previous empirical model based on in situ data. It is also revealed that the subsolar magnetopause can move with speeds of 100–200 km s^{-1} in response to marked dynamic pressure changes, and during periods of stable dynamic pressure can fluctuates with speeds of up to 50 km s^{-1}.

Citation: Hosokawa, K., S. Taguchi, S. Suzuki, M. R. Collier, T. E. Moore, and M. F. Thomsen (2008), Estimation of magnetopause motion from low-energy neutral atom emission, *J. Geophys. Res.*, *113*, A10205, doi:10.1029/2008JA013124.

1. Introduction

[2] The location of the magnetopause, the boundary separating magnetospheric plasma from the solar wind, is one of the most important parameters in the study of energy transfer from the solar wind to the magnetosphere. If closed magnetic flux is opened and transfered from the dayside to the nightside through reconnection, the magnetopause moves closer to the Earth. That is, the past history of the creation and destruction of open magnetic flux within the magnetosphere can be associated with the magnetopause location [e.g., *Milan et al.*, 2004]. In such sense, the location of the dayside magnetopause could be a very useful proxy for monitoring how solar wind energy is transfered to the magnetosphere.

[3] The magnetopause has been observed through in situ measurements of magnetopause crossings since the early 1960s. In most of the early works, the dynamic pressure of the solar wind was employed as the sole factor defining the location of the magnetopause [e.g., *Shield*, 1969]. In later work, however, *Fairfield* [1971] revealed the comparable importance of the north-south component of the interplanetary magnetic field (IMF) orientation for defining the location of the magnetopause. Much of the research conducted in the 1990s [*Roelof and Sibeck*, 1993; *Petrinec and Russell*, 1996; *Shue et al.*, 1997, 1998] developed empirical models of the magnetopause location as functions of the solar wind dynamic pressure and the north-south component of the IMF using large in situ data sets of magnetopause crossings. *Shue et al.* [1998] applied some of the empirical models to actual observations and suggested that the position of the magnetopause is predictable to a certain extent by the empirical models. However, these models are basically steady state models. If we intend to reproduce temporal variations of the magnetopause by using the models, we have to assume that the magnetopause responds instantaneously to variations of the solar wind. In reality, however, the response of the magnetopause to the solar wind drivers is not instantaneous. Thus, to understand the motion of the magnetopause in more detail, it remains necessary to develop an analytical technique by which the magnetopause position can be tracked based on substantial observations.

[4] It has recently been demonstrated that during periods of relatively high solar wind flux, neutral atom emissions are detected by the Low-Energy Neutral Atom (LENA) imager [*Moore et al.*, 2000] on board the Imager for Magnetopause-to-Aurora Global Exploration (IMAGE) spacecraft to be coming from the general direction of the

[1]Department of Information and Communication Engineering, University of Electro-Communications, Tokyo, Japan.
[2]NASA Goddard Space Flight Center, Greenbelt, Maryland, USA.
[3]Los Alamos National Laboratory, Los Alamos, New Mexico, USA.

Copyright 2008 by the American Geophysical Union.
0148-0227/08/2008JA013124

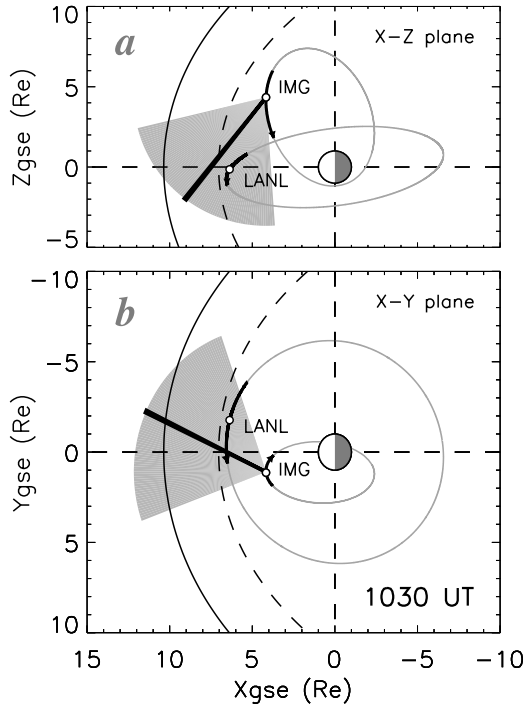

Figure 1. Orbits of IMAGE and LANL-01A spacecraft during the interval of interest in (a) GSE *X-Z* and (b) *X-Y* planes. Open circles denote spacecraft position at 1030 UT. Shaded areas denote FOV of LENA looking into the neutral atom emission of equatorial magnetosheath origin. In Figure 1a, spin angle sectors of 40° to 120° are displayed, spin angle of 80° being shown as black solid line. In Figure 1b, polar angle sectors of −45° to 45° are displayed, polar angle of 0° is shown as black solid line. Solid and dashed curves represent the positions of the magnetopause predicted by the model of *Shue et al.* [1998] immediately prior to 1000 UT (before the enhancement of the LENA emission) and at 1030 UT (time of most compressed magnetopause), respectively.

subsolar magnetopause [*Collier et al.*, 2001b; *Taguchi et al.*, 2004; *Collier et al.*, 2005]. Neutral atoms from the magnetosheath may include components with higher energies than the nominal energy upper limit of LENA (300 eV). Such high-energy components can sputter negative ions with much lower energies from the tungsten conversion surface of LENA [*Collier et al.*, 2001a], allowing LENA to respond to incident neutrals with energies of up to a few keV [*Moore et al.*, 2003]. It has thus been found possible to analyze ENAs originating from magnetosheath ions (typical energy is ≈keV).

[5] When the dayside magnetopause is highly compressed, magnetosheath ions can penetrate into the region of higher exospheric hydrogen neutral density. In such cases, magnetosheath ions interact with exospheric neutrals more effectively, producing an elevated flux of energetic neutral atoms (ENAs). *Taguchi et al.* [2004] estimated that ENA emissions from the general direction of the subsolar magnetopause toward the spacecraft position increases by a factor of 3 at subsolar distances of 6.6 R_E to 5.6 R_E. The detailed response of the neutral atom flux to magnetopause compression was examined by *Collier et al.* [2005] as part of a comparison of the intensity of neutral atom emissions traveling from the general direction of the subsolar magnetopause with the subsolar distance of the magnetopause predicted by the model of *Sibeck et al.* [1991]. *Collier et al.* [2005] suggested that ENA emissions are highly sensitive, probably in a nonlinear manner, to the subsolar distance of the magnetopause.

[6] The formula of ENA flux used by *Collier et al.* [2005] includes two free parameters that determine the size of the ENA source region. In the present paper, these two parameters are calculated by examining LENA snapshots in detail, and using information on one magnetopause crossing of the geosynchronous LANL-01A spacecraft. Using these new parameters, the temporal variation in subsolar distance over a period of more than 1 h is determined.

2. Observations

2.1. Overview

[7] Figure 1 shows an overview of the spacecraft orbits between 0900 and 1200 UT on 13 April 2001 in the GSE *X-Z* (Figure 1a) and *X-Y* (Figure 1b) planes. The IMAGE spacecraft was located over the Northern Hemisphere and was in a descending phase from apogee over the North Pole. Shaded areas denote the FOV of LENA looking into the neutral atom emissions of equatorial magnetosheath origin. In the top panel, spin angle sectors of 40° to 120° are displayed, with the spin angle of 80° being shown as a black solid line. In the bottom panel, polar angle sectors of −45° to 45° are displayed, with the polar angle of 0° shown as a black solid line. LANL-01A was located on the prenoon side (≈11 MLT at 1030 UT). The period from 0955 to 1106 UT is considered here, during which IMAGE/LENA observed enhanced neutral atom emissions from the direction of the low-latitude magnetosheath.

[8] The Advanced Composition Explorer (ACE) spacecraft provides information on the solar wind far upstream of the Earth. In the study period, the solar wind dynamic pressure varied considerably and the location of the magnetopause is expected to have fluctuated accordingly. Two predictions of the magnetopause position according to the model of *Shue et al.* [1998] are shown in the figure; that before enhancement of LENA emissions (before 1000 UT; solid curve), and that corresponding to the most compressed magnetopause (1030 UT; dashed curve) during the interval of interest.

2.2. Solar Wind and IMF

[9] Observations by the magnetometer (MAG) and solar wind electron, proton, and alpha monitor (SWEPAM) instruments on board the ACE spacecraft are presented in Figure 2. At 1030 UT on 13 April 2001, the spacecraft was located near $[X_{gse}, Y_{gse}, Z_{gse}] \approx [221.7\ R_E, -0.8\ R_E, -21.4\ R_E]$. The solar wind velocity was largely steady at around 800 km s^{-1} throughout the interval. The time lag from ACE to the dayside magnetopause is estimated to be 30 min from the ACE X_{gse} location of 221.7 R_E and a solar wind speed of ≈800 km s^{-1}. This time lag is consistent with the correspondence between a sharp increase in the solar wind dynamic pressure from 3 to 15 nPa and the positive sudden impulse (SI$^+$) [*Araki*, 1994] in the *H* component of the SYM index (Figure 2f) [*Iyemori and Rao*, 1996]. The

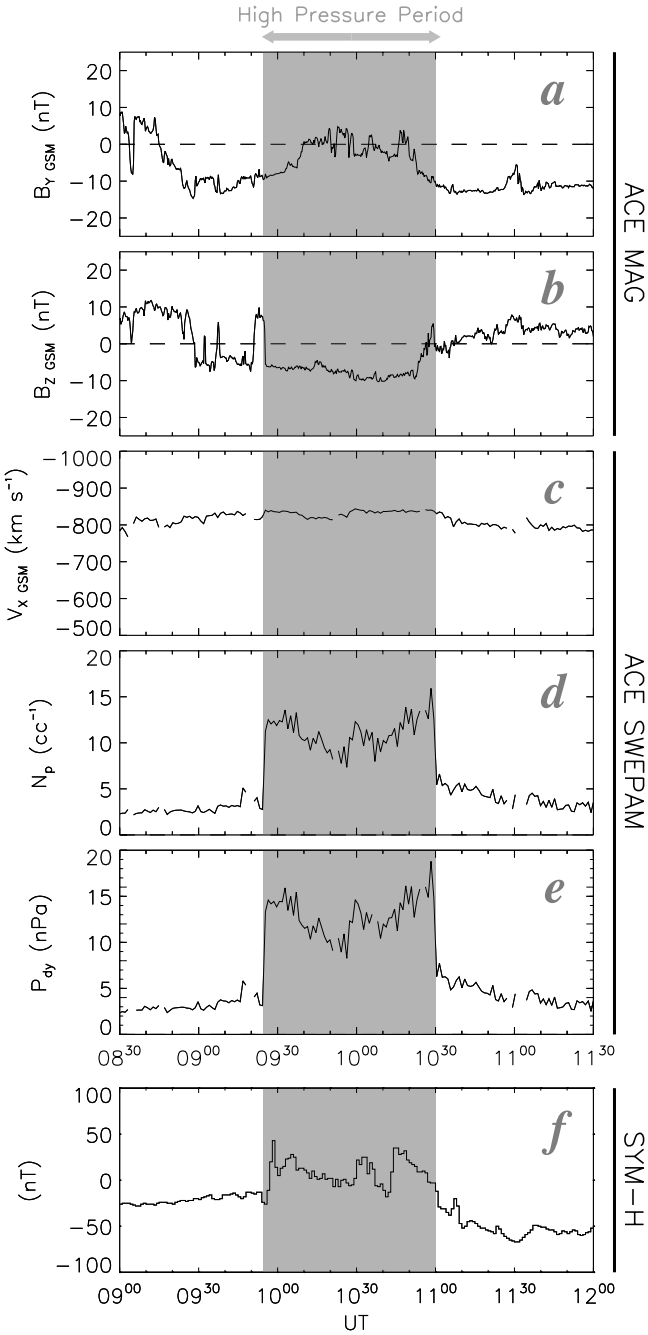

Figure 2. (a–e) Solar wind and interplanetary magnetic field conditions measured by the SWEPAM and MAG instruments on board the ACE spacecraft time-shifted to the dayside magnetopause. (f) SYM-H index. Shaded area denotes period of high solar wind pressure in which the motion of the magnetopause is estimated.

ACE data are thus shifted by 30 min in Figure 2 (time axis at the position of ACE is shown between Figures 2e and 2f). After the SI^+ at 0955 UT, the dynamic pressure remained high for approximately 1 hour and then decreased suddenly to 5 nPa at 1100 UT. This 1 hour interval of high solar wind pressure is referred to hereafter as the high-pressure period, during which the B_z component of the IMF was predominantly southward between −7 and −10 nT.

2.3. ENA Measurement

[10] Figure 3 shows the LENA spectrogram from 0900 to 1200 UT on 13 April 2001. The IMAGE spacecraft spins in the reverse cartwheel mode, that is, the spin vector is anti-parallel to the orbital angular momentum vector. The FOV of the LENA instrument spans ±45° with respect to the plane perpendicular to the spacecraft spin axis, and is divided into 12 polar sectors (7.5° resolution). As the spacecraft spins, the instrument sweeps out 360° in the spin direction, which is divided into 45 spin sectors (8° resolution). One complete scan, covering 90° (in the polar angle direction) × 360° (in the spin angle direction), is obtained in a spacecraft spin period of 2 min. The count rate shown in the figure is summed over the 12 polar sectors. The bright signal starting at approximately 120° in the spin angle and running along the time axis represents a neutral atom flux enhancement in the direction of the Sun (i.e., Sun signal [*Moore et al.*, 2001; *Collier et al.*, 2001a, 2003]).

[11] Shortly after onset of the high-pressure period, strong enhancements in the hydrogen count rate can be identified. These enhancements originated from a wide range of spin angles, but appear to be most intense in the spin angle sectors looking into the direction between the Earth and the Sun signal. The magnetopause location is estimated later in this paper from ENA observations from these spin angle sectors, which generally look into the dayside low-latitude magnetosheath (see Figure 1a). Relatively weak enhancements can also be seen at spin angles higher than that of the Sun signal. These features are interpreted as the product of a charge-exchange process between ions injected into the cusp and exospheric hydrogen neutrals [*Taguchi et al.*, 2004, 2005, 2006; *Murata et al.*, 2007].

[12] As shown in Figure 1, IMAGE was located inside the magnetopause as estimated by the model of *Shue et al.* [1998]. However, the model magnetopause is sometimes not accurate at high latitudes. Thus, IMAGE might be in the magnetosheath during the period under study. This is actually the case for the interval studied by *Collier et al.* [2005]. In such case, low-energy solar wind plasma surrounds the spacecraft and the LENA instrument observes energetic neutrals from all directions. During the interval presented, however, neutral atoms came mainly from the general direction of the dayside magnetosheath, which suggests that the spacecraft was not in the magnetosheath but inside the magnetopause. Our method is based on the one proposed by *Collier et al.* [2005], who have demonstrated that the method is valid if the spacecraft is situated in the magnetosheath. Thus, even if the spacecraft was in the magnetosheath during the interval of current study, it does not affect the main conclusion of this paper.

[13] A sequence of two-dimensional hydrogen LENA images taken every 2 min during the high-pressure period (0955–1106 UT) is presented in Figure 4. At 0955 UT (Figure 4a), before the increased solar wind dynamic pressure had reached the magnetopause, neutral atom emissions were weak. At 0957 UT (Figure 4b), however, enhanced emissions can be first detected at spin angles between 70° and 120°. Fluctuating but elevated emissions from this angle range can be observed continuously until 1100 UT (63 min later). At 1017 UT (Figure 4c), enhanced emissions emerged at a spin angle of 80°. The emissions at spin angles between 60° and 120° again became more

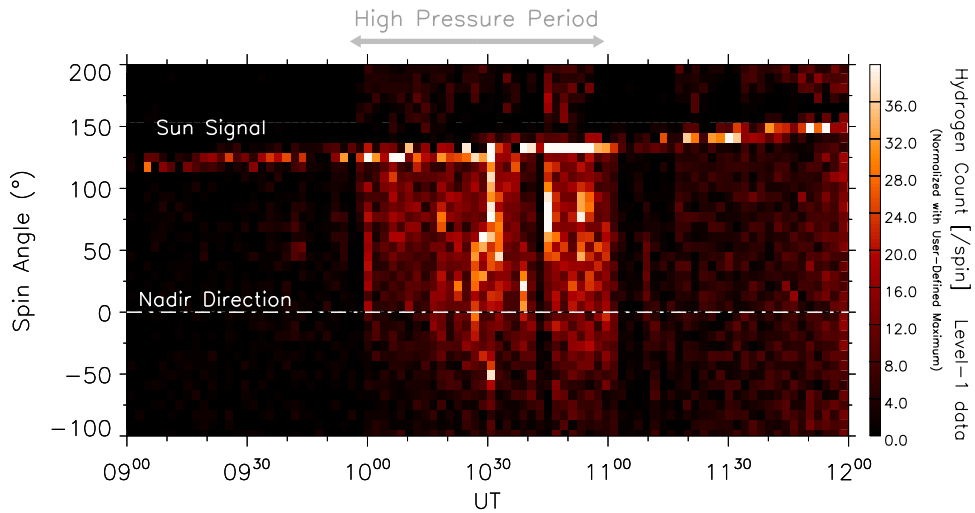

Figure 3. LENA spectrogram (spacecraft spin angle versus UT). Background-adjusted hydrogen count rates (over entire energy range) are obtained by summing over the 90° polar FOV (color coded). Horizontal dash-dotted line denotes the earthward (Nadir) direction.

intense at 1029 UT (Figure 4d), but then underwent sudden weakening at 1042 UT (Figure 4e). At 1044 UT (Figure 4f), enhanced emissions were re-established at spin angles between 60° and 100°. The emissions then weakened somewhat, but increased once more at 1052 UT (Figure 4g). It will be demonstrated later (in section 3.3) that the emissions are enhanced in response to the inward motion of the magnetopause. The emissions from the general direction of the dayside low-latitude magnetosheath disappeared completely by 1102 UT (Figure 4j).

2.4. Geosynchronous Magnetopause Crossings

[14] During the interval of interest, the LANL-01A geosynchronous spacecraft was located on the dayside and detected two major magnetopause crossings. Figure 5 shows ion and electron color spectrograms of the magnetospheric plasma analyzer (MPA) instrument [*McComas et al.*, 1994] from 0955 UT to 1105 UT (data are not available until 1007 UT). In two intervals, 1028–1038 UT and 1042–1100 UT, intense fluxes of electrons with energies below 1 keV and ions with energies of ≈100 eV to 10 keV are apparent. These intervals can be interpreted as the times during which LANL-01A was in the magnetosheath [e.g., *Ober et al.*, 2002]. During these two intervals, the subsolar magnetopause was located inside the geosynchronous orbit at a distance of 6.6 R_E, which will be compared with the magnetopause location estimated from the ENA observations. Note that the MLT of LANL-01A was ≈1100 MLT at the time of the first major magnetopause crossing (1028 UT). The spacecraft was close enough to local noon to do the comparison as if it was located at local noon.

3. Deduction of Magnetopause Motion From ENA

3.1. Low-Latitude Sheath ENA Emission

[15] As presented above, the LENA imager on board the IMAGE spacecraft observed enhanced ENA flux originating from the direction of the low-latitude magnetosheath during the high pressure period. These low-latitude sheath emissions have been examined in several recent studies [*Collier et al.*, 2001b; *Taguchi et al.*, 2004; *Collier et al.*, 2005]. *Collier et al.* [2005] proposed that the ENA flux observed by the spacecraft Φ_n is proportional to the solar wind flux Φ_{sw}, the density of exospheric neutrals at the nose of the magnetopause n_H, and the effective line-of-sight l_{los}. Φ_n is also inversely proportional to the square of the distance from the source to the spacecraft r. This implies that when a high-pressure solar wind pushes the magnetopause closer to the Earth, Φ_n should be enhanced due to contributions from increased Φ_{sw}, higher n_H resulting from the compressed magnetosphere, and decreased r. Furthermore, when the spacecraft views the low-latitude magnetosheath from higher latitude, the tangential viewing angle increases the effective l_{los} through the ENA source. This factor also contributes to the enhancement of low-latitude sheath emissions. Note that all of the above factors affecting Φ_n, excluding Φ_{sw}, are dependent on the subsolar distance of the magnetopause R_{mp}, allowing Φ_n to be described as a function of R_{mp}. The value of R_{mp} will be estimated later from the LENA measurement of Φ_n.

3.2. ENA Flux Model

[16] The mathematical expression for Φ_n as a function of R_{mp} is derived here using a slightly modified version of the model first proposed by *Collier et al.* [2005]. The X position of the IMAGE spacecraft, assumed to be zero in the model by *Collier et al.* [2005], is introduced here as a variable. Figure 6 shows a schematic illustration of the model in the noon-midnight plane in GSM coordinates. For simplicity, this model assumes that the source of the ENA flux observed at the spacecraft position is a small region of thickness l and characteristics size d at the nose of the magnetopause. The location of the IMAGE spacecraft is given by [X_{im}, Z_{im}]. The flux of neutral atom emissions observed by the spacecraft (Φ_n) is then given by

$$\Phi_n = \Phi_{sw} \cdot \sigma \cdot n_H \cdot l_{los} \cdot \left(\frac{d}{r}\right)^2, \qquad (1)$$

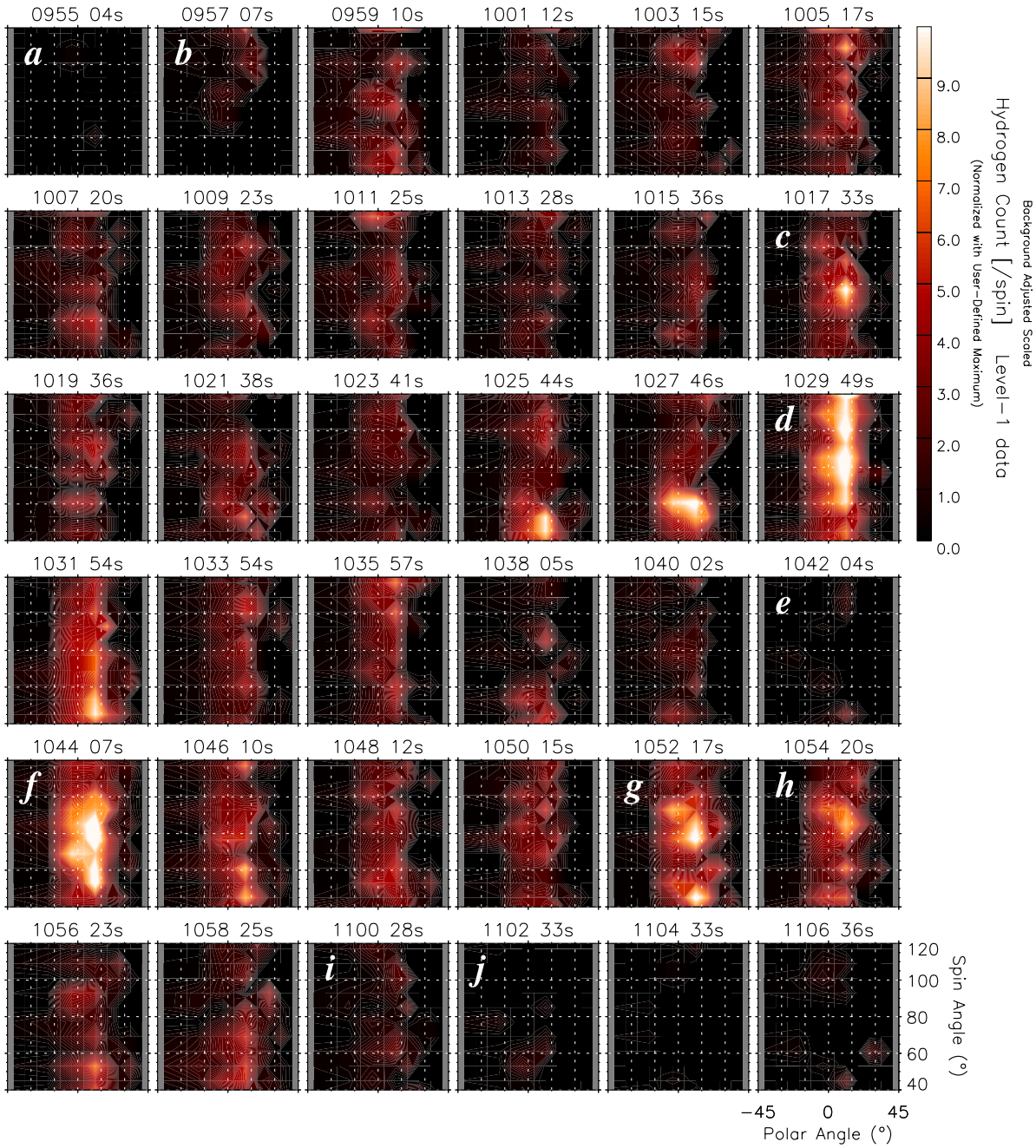

Figure 4. Sequence of two-dimensional low-energy hydrogen ENA images from 0955 UT to 1106 UT. Background-adjusted hydrogen count rates are plotted according to polar angle and spin angle. Data for spin angles of 40–120° are shown. Some of the panels are labeled to aid the discussion in the text.

where σ is the charge-exchange cross-section [*Collier et al.*, 2005]. In this equation, n_H, l_{los}, and r have a nonlinear relationship with R_{mp}, while Φ_{sw} and σ are independent of R_{mp}. According to the model presented by *Rairden et al.* [1986], n_H is given by

$$n_H = n_{10}\left(\frac{10}{R_{mp}}\right)^{2.91}, \tag{2}$$

where n_{10} is the exospheric number density at 10 $R_E \approx$ 10 cm^{-3}. The effective l_{los} is expressed by

$$l_{los} = \frac{l}{\cos\theta} = \frac{lr}{R_{mp} - X_{im}}, \tag{3}$$

where θ ($<\pi/2$) is the angle between the GSM x axis and the line-of-sight vector of the LENA imager (Figure 6).

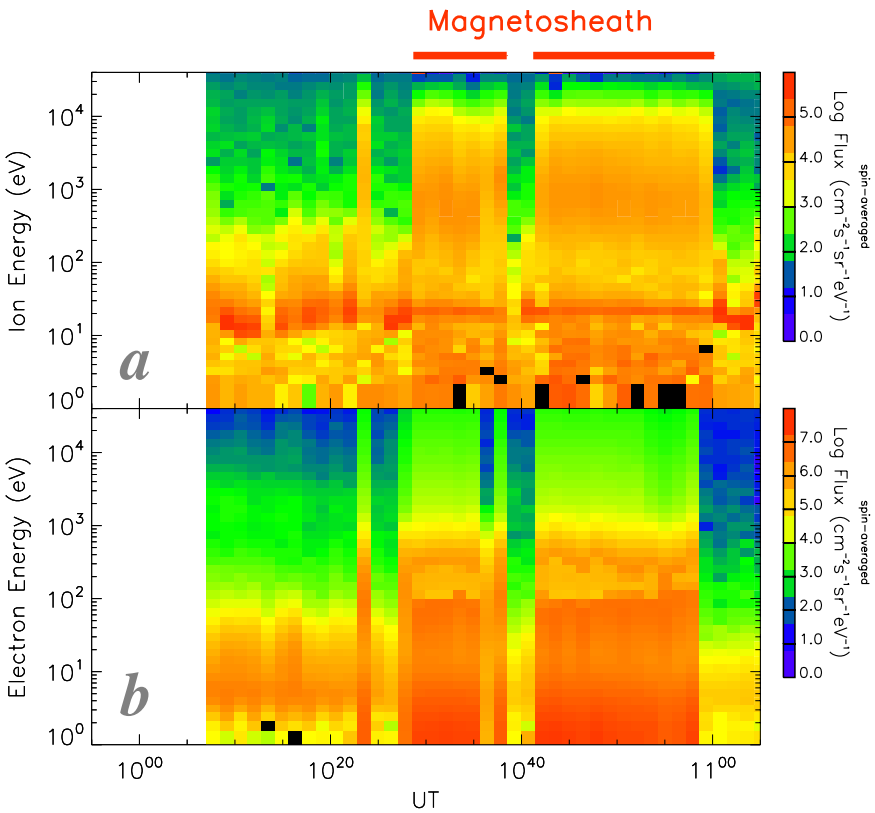

Figure 5. Ion and electron energy-time spectrograms observed by the MPA instrument on board the LANL-01A spacecraft from 0955 UT to 1105 UT. Data from this instrument became available shortly after onset of the high-pressure period (1007 UT). The two intervals in which the spacecraft was in the magnetosheath are indicated by red bars.

The distance from the source to the spacecraft r is given by

$$r = \sqrt{(R_{mp} - X_{im})^2 + Z_{im}^2}. \tag{4}$$

Finally, the neutral atom flux observed by the spacecraft can be expressed by

$$\Phi_n = \Phi_{sw} \cdot \sigma \cdot n_{10} \cdot \left(\frac{10}{R_{mp}}\right)^{2.91} \cdot d^2 \cdot l \cdot \frac{1}{R_{mp} - X_{im}} \cdot \frac{1}{\sqrt{(R_{mp} - X_{im})^2 + Z_{im}^2}}. \tag{5}$$

The flux of flow in the magnetosheath Φ_{sw} can be approximated by that observed by ACE in the upstream solar wind, and σ can be assumed to be approximately 2×10^{-15} cm^2 [*Collier et al.*, 2005; *Taguchi et al.*, 2005]. R_{mp} can then be calculated from the observed Φ_n assuming values of the scale size d and thickness l of the ENA source region.

3.3. Magnetopause Position

[17] The spatial scale of the ENA source region at the subsolar magnetopause (characteristic size d along the surface of the magnetopause and thickness l along the GSM x axis) is a necessary input for the estimation of R_{mp}. Here, we try to estimate the spatial scale of the ENA source region (d) by projecting the ENA emissions to the magnetopause model of *Shue et al.* [1998] along the line-of-sight of the LENA imager. Figure 7 shows two-dimensional ENA images for times at which the low-latitude sheath emissions were clearly observed. Irrespective of the subsolar distance, the emissions originate from the small region slightly poleward of the nose of the magnetopause. Strongest magnetosheath ENA emissions can be observed from a region where the magnetosheath flow line is anti-parallel to the line-of-sight vector of the LENA imager. The magnetosheath flow is generally poleward along the surface of the magnetopause. Thus, the anti-parallel condition makes the LENA imager to favor polar viewing and strong ENA emission appears slightly poleward of the nose of the magnetopause.

[18] It is difficult to estimate the spatial extent of the source region (d) uniquely. Thus, we employ three different ENA source regions and estimate the magnetopause location individually for each case. Three ENA source regions are shown as rectangles in Figure 7. The red, green and blue rectangles represent the largest, medium and smallest source regions, respectively. The value of d^2 can therefore be set to 25 R_E^2 for largest case, 10 R_E^2 for medium, and 2 R_E^2 for smallest. In each case, ENA flux obtained within the rectangle is used as an input for Φ_n in equation (5).

[19] As the thickness l cannot be estimated from actual observations because the observed ENA flux is an integra-

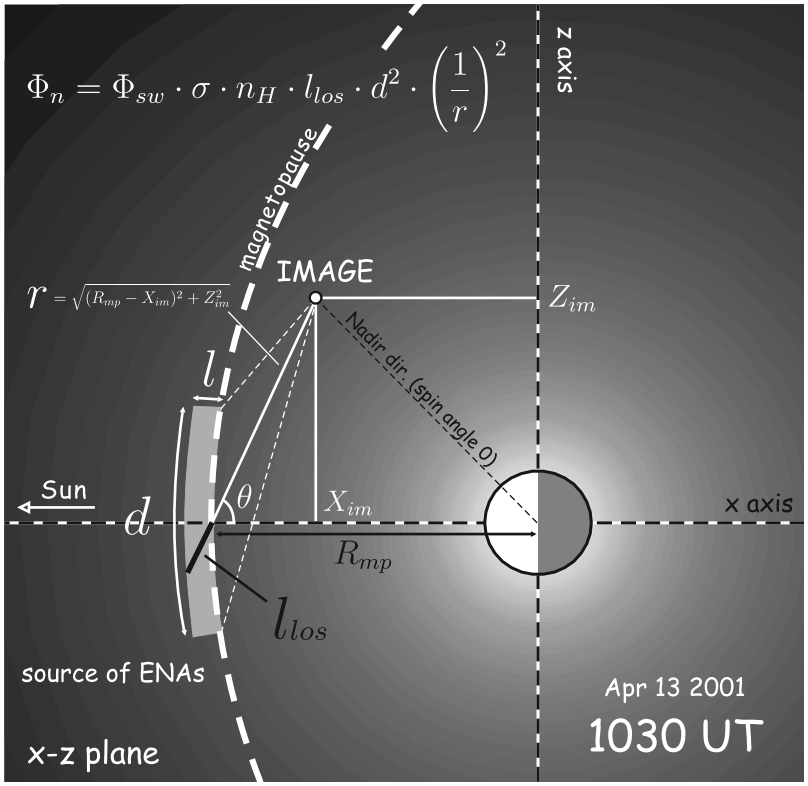

Figure 6. Schematic illustration of the model of ENA source employed for estimation of magnetopause position from ENA measurements.

tion of all ENA emissions along the line-of-sight of the imager, the in situ observations of geosynchronous magnetopause crossings by LANL-01A are consulted in order to obtain an approximation. The LANL spacecraft crossed the magnetopause at 1028 UT and entered the magnetosheath. At this time, the subsolar magnetopause should have been located at 6.6 R_E. Thus, setting $R_{mp} = 6.6\ R_E$, with $d^2 = 10\ R_E^2$ (medium case) and $\Phi_{sw} = 10.4 \times 10^{12}\ \mathrm{m}^{-2}\ \mathrm{s}^{-1}$ from ACE solar wind data corresponding to the LANL-01A observation at 1028 UT, Equation (5) gives $l = 0.30\ R_E$ ($\approx$2000 km). For the cases of largest and smallest d values, we estimated l with the same procedure and obtained almost similar values. Thus, $l = 0.30\ R_E$ is employed in the calculation for all cases.

[20] Figure 8a shows the variation in Φ_n calculated using the nominal instrument parameters for LENA: a neutral hydrogen detection efficiency at solar wind energies of 6.4×10^{-5} [*Collier et al.*, 2001a], an entrance aperture of 1 cm^2, and integration time of 2.7 s. The magnetopause subsolar distance estimated using Equation (5) and the ion spectrogram observed by the MPA instrument of the LANL-01A spacecraft are also shown (Figures 8b and 8c). As mentioned in the previous part of this section, we employed three different d values for the calculation of R_{mp}. Thus, we obtained three different time series of R_{mp}. Here, the magnetopause subsolar distance R_{LENA} is estimated from averaging the three R_{mp} values. Error is also estimated from the deviation of the largest and smallest R_{mp} values from average. The present result, R_{LENA}, is compared with the magnetopause subsolar distance predicated by the model of *Shue et al.* [1998].

[21] At 0955 UT, before the arrival of the high-pressure solar wind, R_{LENA} was near the nominal position of the magnetopause (>10 R_E). Two minutes later (0957 UT), the solar wind pressure increased from 3 to 15 nPa, causing R_{LENA} to promptly decrease to close to 8 R_E. For approximately 30 min, R_{LENA} remained relatively steady around the geosynchronous orbit. At 1028 UT, R_{LENA} further decreased to 5.5 R_E and then remained inside the geosynchronous orbit for 10 min. This time (1028 UT) corresponds to the measured magnetopause crossing of the LANL-01A spacecraft. It is not surprising that R_{LENA} agrees with the LANL-01A observation at 1028 UT because our model determines the value of thickness l using the LANL-01A observation at this time. Importantly, however, R_{LENA} continues to remain consistent with the LANL-01A observations after this time. At 1036 UT, R_{LENA} moved away from the geosynchronous orbit, increasing to approximately 11 R_E in 4–6 min. At 1042 UT, R_{LENA} crossed the geosynchronous orbit once again, and then remained inside the 6.6 R_E boundary for 15 min. The LANL-01A spacecraft also crossed the magnetopause at around 1042 UT and then stayed within 6.6 R_E for 20 min. After the solar wind dynamic pressure decreased to the original value, $\approx$5 nPa (1100 UT), R_{LENA} gradually increased to >10 R_E. The remarkable consistency between R_{LENA} and the geosynchronous observation demonstrates that the motion of the magnetopause was successfully tracked for more than 1 hour, which has never before been achieved through in situ spacecraft observations. Note that R_{Shue} never falls within the geosynchronous orbit, whereas both R_{LENA} and LANL-01A exhibit very similar variations throughout this

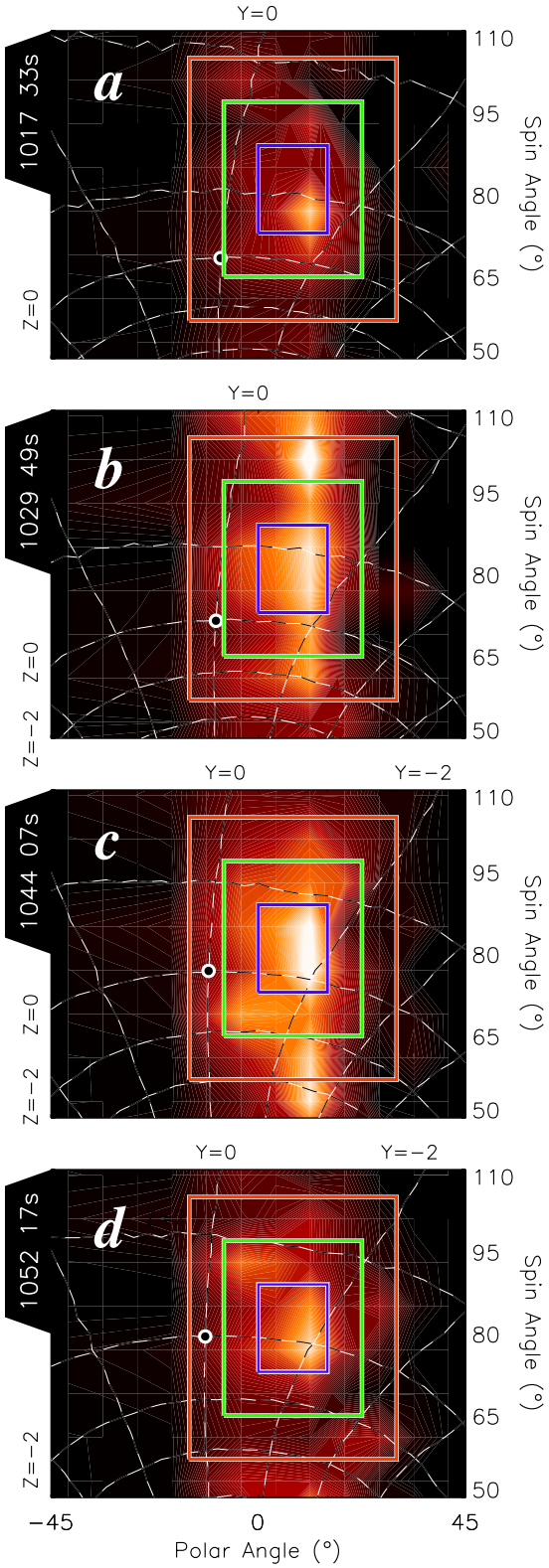

Figure 7. Two-dimensional low-energy hydrogen ENA images for selected times of observed low-latitude sheath emission. Dashed lines denote the projection onto the magnetopause model of *Shue et al.* [1998], showing contours of constant Y_{gsm} and Z_{gsm}. The black dot denotes the nose of the magnetopause. The rectangles indicate the area of ENA emissions employed for calculation of magnetopause position.

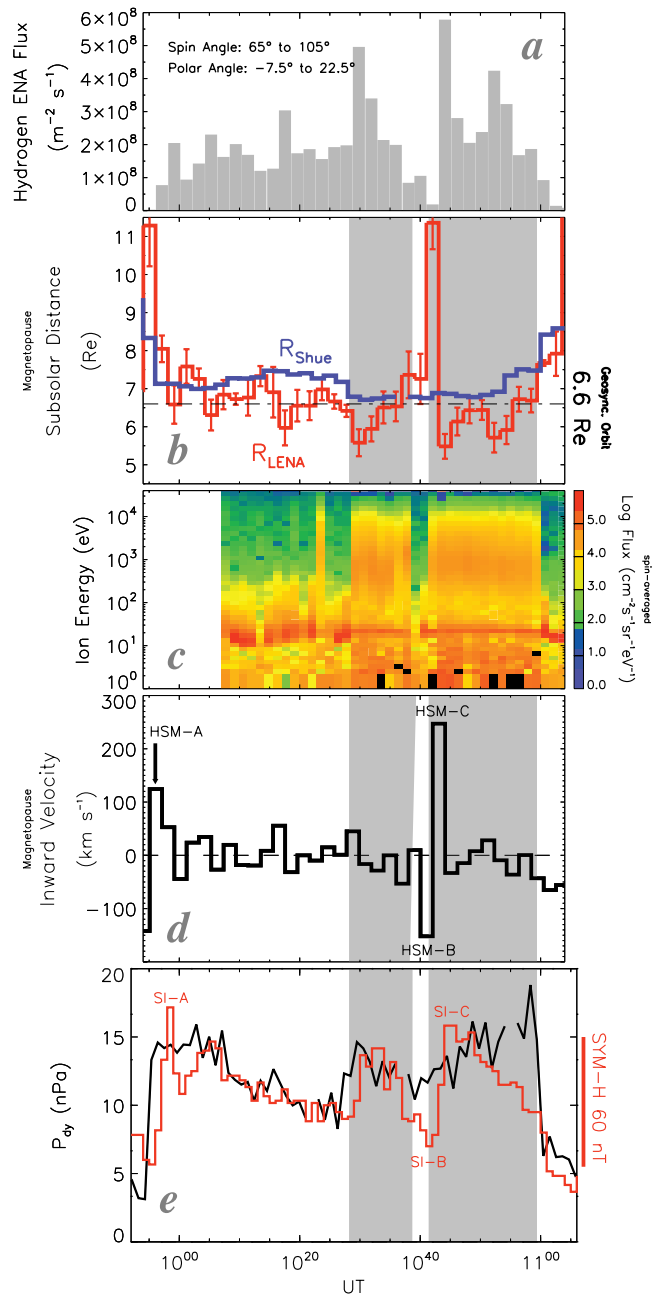

Figure 8. (a) Time series of ENA flux observed in the direction of the equatorial magnetosheath Φ_n. (b) Estimated magnetopause subsolar distance R_{LENA} during the high-pressure period (red line). The blue line denotes the magnetopause subsolar distance predicted by the model of *Shue et al.* [1998] (R_{Shue}), and the horizontal dash-dotted line denotes the geosynchronous orbit (6.6 R_E). (c) Ion spectrogram recorded by the MPA instrument on board the LANL-01A spacecraft. The intervals in which the magnetopause was apparently located inside the geosynchronous orbit are shaded. (d) Inward velocity of magnetopause derived from the modeled magnetopause position. (e) Variation in solar wind dynamic pressure (black line) and SYM-H index (red line).

interval. This result implies that, at least in the present case, the technique employed here provides a better estimation of magnetopause motion than the model of *Shue et al.* [1998], although we have to remind again that the model of *Shue et al.* [1998] is a steady state model and should not be used for reproducing dynamic behavior of the boundary.

3.4. Rapid Motion of Magnetopause

[22] The velocity of the inward/outward motion of the dayside magnetopause, derived from the time series of R_{LENA} (Figure 8b), is shown in Figure 8d. Here, we estimated the velocity of the magnetopause by calculating the difference of the magnetopause location between consecutive data points and dividing it by the sampling interval of 120 s. The estimated velocities of the magnetopause are typically between -50 and 50 km s^{-1} in this interval. These values are very close to those derived from recent multi-spacecraft observations of magnetopause motion, such as those conducted by the Cluster spacecraft [*Halland et al.*, 2004].

[23] The present result also demonstrates that the speed of magnetopause motion sometimes reaches the order of 100 km s^{-1}. Three such events are identified in Figure 8d (denoted A, B, C). These high-speed events can be compared with the variation in solar wind dynamic pressure as shown in Figure 8e based on ACE observations and the SYM-H index, which is used as a proxy for solar wind pressure enhancements at the dayside magnetopause. Three sudden increases in SYM-H occurred during the high-pressure period. The first increase associated with SI-A pushed the magnetopause from its nominal position ($\approx$11 R_E) to approximately 8 R_E and caused the first high-speed motion (HSM) event, reaching a speed of 130 km s^{-1}. The next pressure increase at 1028 UT (not marked) compressed the magnetosphere further inward, causing the magnetopause to cross the geosynchronous orbit. The speed of the magnetopause motion in this case was lower than in the other movements ($\approx$40 km s^{-1}), presumably because the magnetopause was already compressed to some extent before this pressure enhancement. Ten minutes later, the dynamic pressure of the solar wind impinging on the dayside magnetopause decreased rapidly. This change, which can be clearly seen in the SYM-H index (SI-B), caused a very rapid outward motion of the magnetopause (HSM-B), reaching speeds higher than 100 km s^{-1}. The solar wind dynamic pressure increased again immediately following this motion (corresponding variation in SYM-H is SI-C), causing the magnetopause to move inward at approximately 200 km s^{-1}. Note that, in the later part of the interval (after 1030 UT), rapid variations seen in the LENA, LANL-01A and ground SYM-H index are not so clear in the solar wind data. This is perhaps due to the fact that the solar wind structure changed significantly as it propagates from the location of ACE to the dayside subsolar magnetopause.

4. Discussion

[24] The model presented in this paper takes LENA total counts as an input, but does not consider the temporal variations in the direction of the enhanced emissions. This means that the model does not explicitly take into account the magnetosheath flow lines, which may favor polar viewing, as stated by *Collier et al.* [2005]. However, the narrow ENA source region of the event to which the present model was applied (i.e, $l \ll d$), effectively constrains the model to the local magnetosheath flow lines. With the ENA source region located at R = 6.6 R_E and LENA looking into a region with dimensions of $\sqrt{10}R_E \times 0.3\ R_E$, the FOV is roughly 25° in the spin angle plane, corresponding to 3 spin angle bins of LENA. This is in agreement with the modeling results of *Taguchi et al.* [2004], who showed that the enhanced low-latitude sheath emissions detected by LENA are seen in 3 spin angle bins taking into account the sheath flow direction.

[25] Before comparing the current result with past publications, we must discuss its reliability. Since the measured count rates are fairly low, one may suspect that the original LENA data contain Poisson type noise. If the noise dominates temporal variation of the LENA count, the estimated magnetopause motion, especially its variation in short temporal scale, is meaningless. However, we have concluded that Poisson noise cannot affect our final results considerably for the following two reasons: (1) we have preprocessed the original LENA data very carefully. First, the background could rate is estimated and subtracted from the original data. In this step, the background count rate is derived from the count level between the hydrogen peak and the oxygen peak in the time-of-flight spectra. Second, we have filtered out isolated counts in spin-polar angle frame, which is corresponding to an elimination of Poisson noise. Thus, we have removed Poisson type noise as much as possible before examining the data, (2) we used the sum of the LENA counts from the spin-polar angle sectors corresponding to the assumed ENA source regions. This includes LENA spin angles of 65° to 97° and polar angles of $-7.5°$ to 22.5° for the medium size ENA source region case. Even if the LENA data after the preprocessing procedure still contains some Poisson noise, this integration process reduces the possible contribution of noise to the estimated results, because the noise would appear almost randomly in each polar-spin angle sector.

[26] The present results reveal that the subsolar magnetopause can move at speeds of 100–200 km s^{-1} in response to sudden marked changes in solar wind dynamic pressure, and fluctuate at speeds of 50 km s^{-1} or less during periods of stable dynamic pressure. A similar high speed motion and fluctuation of the magnetopause were reported by *Dunlop et al.* [2001, 2002] on the basis of Cluster data. *Dunlop et al.* [2001, 2002] also pointed out that the magnetopause speed can change dramatically over timescales of a minute or less. Our results are basically consistent with their results and may not be so surprising. However, we can monitor the motion of the magnetopause almost continuously as long as LENA can observe significant ENA flux from the magnetosheath when the solar wind pressure is high enough. This could be a great advantage of our method over the in situ spacecraft observations.

[27] During the event examined in the present paper, IMF B_z remained steady between -6 and -8 nT. The rapid motion of the magnetopause (>100 km s^{-1}) has therefore been attributed to the effect of sharp variations in solar wind dynamic pressure. However, *Collier et al.* [2005] reported an ENA flux event on 18 April 2001 during which the solar

wind dynamic pressure was approximately constant. In that case, the ENA flux was suggested to be extremely sensitive to changes in the IMF B_z component. In addition, variation of the IMF B_y is another possible factor controlling the amount of neutral flux coming from the direction of the dayside equatorial magnetopause. Actually, the IMF was varying back and forth during the interval under study (Figure 2). Although it is difficult to find general correlation between variations of IMF B_y and magnetosheath ENA flux, the change of IMF B_y (i.e. change of reconnection rate due to the variation of the IMF clock angle) may cause variations which are not associated with the solar wind pressure changes. A search for events in which both dynamic pressure and IMF B_y, B_z effects can be quantified separately is therefore a natural next step in the study of magnetopause behavior.

[28] It should be noted that we may be able to apply the current method to the ENA observations around other planets such as Mars. Recent observation by Mars Express demonstrated that similar ENA emission, so-called ENA jet [*Futaana et al.*, 2006a], comes from the Martian magnetic pileup boundary, which is very similar to the magnetopause of the Earth. The generation mechanism of the ENA jet is still under debate. However, one of the possible explanations is charge exchange process between the shocked solar wind protons and Martian exospheric neutrals [*Holmstrom et al.*, 2002]. The Martian ENA jet and ENA emissions from the Earth's magnetosheath have some common characteristics. We presented that the estimated thickness of the ENA source region is very small (l = 0.30 R_E) and that the emissions extend roughly 25° in the spin angle plane. The Martian ENA jet is also known to be highly directional flow from the subsolar region [*Futaana et al.*, 2006b]. This similarity may suggest that these two types of ENA emissions have a common generation mechanism. Moreover, the intensity of the Martian ENA jet exhibits oscillative behavior whose timescale is approximately 5 min [*Grigoriev et al.*, 2006]. This oscillation may be due to temporal variations of the solar wind dynamic pressure or small scale structures in the vicinity of the boundary. Our results also show that the estimated magnetopause position fluctuates with an order of a few minutes. The similarities of the Martian ENA jet and the ENA emissions from the Earth's magnetosheath suggest a possibility of some comparative studies of the ENA around Earth-type bodies.

[29] We have demonstrated that the method presented in this paper is very powerful for monitoring the motion of the dayside magnetopause. However, the method may not always be applicable for the estimation. In reality, the subsolar distance R_{LENA} shown in Figure 8b may not be correct when the magnetopause is located at its nominal position $\approx$10 R_E and thus the magnetosheath ENA emission is considerably faint. We have not tested the current method to the cases of moderate solar wind conditions. Evaluation of the method for such moderate solar wind cases is intended as a next step.

5. Summary and Conclusion

[30] An algorithm for calculating the subsolar distance of the magnetopause from low-latitude magnetosheath ENA emissions observed by IMAGE/LENA was proposed. Although the algorithm is based on a simple analytical model and includes several assumptions, the predicted variations in subsolar distance during a period of high solar wind dynamic pressure on 13 April 2001 is in remarkable agreement with the geosynchronous magnetopause crossing detected by LANL-01. During this event, the dynamic pressure varied between 3 and 15 nPa, with IMF B_z remaining steady. This model allows the position of the subsolar magnetopause to be tracked for a period of over 1 hour during the event studied, revealing that the dayside magnetopause moves inward across the geosynchronous orbit and fluctuates on short timescales. The present result also demonstrates that the subsolar magnetopause can move with speeds of 100–200 km s^{-1} in response to marked changes in dynamic pressure, and fluctuates during periods of stable dynamic pressure with speeds of up to 50 km s^{-1}.

[31] **Acknowledgments.** This research was supported by a Grant-in-Aid (18540443, Category C) from the Japan Society for the Promotion of Science, and by the IMAGE project (UPN 370-28-20) at the Goddard Space Flight Center. The authors wish to thank N. Ness at the Bartol Research Institute for access to data from the MFI and SWE instruments on board the ACE spacecraft.

[32] Zuyin Pu thanks the reviewers for their assistance in evaluating this paper.

References

Araki, T. (1994), A physical model of the geomagnetic sudden commencement, in *Solar Wind Sources of Magnetospheric Ultra-Low-Frequency Waves*, *Geophys. Monogr. Ser.*, vol. 81, edited by M. Engebretson, K. Takahashi, and M. Scholer, 182 pp., AGU, Washington, D. C.

Collier, M. R., et al. (2001a), Observations of neutral atoms from the solar wind, *J. Geophys. Res.*, *106*, 24,893.

Collier, M. R., et al. (2001b), LENA observations on March 31, 2001: Magnetosheath remote sensing, *Eos Trans. AGU*, *82*(47), Fall Meet. Suppl., Abstract SM41C-05.

Collier, M. R., et al. (2003), Dust in the wind: The dust geometric cross section at 1 AU based on neutral solar wind observations, in *Solar Wind Ten*, edited by M. Velli, R. Bruno, and F. Malara, *AIP Conf. Proc.*, *679*, 790.

Collier, M. R., T. E. Moore, M.-C. Fok, B. Bilkerton, S. Boardsen, and H. Khan (2005), Low-energy neutral atom signatures of magnetopause motion in response to southward B_z, *J. Geophys. Res.*, *110*, A02102, doi:10.1029/2004JA010626.

Dunlop, M. W., et al. (2001), Cluster observes the Earth's magnetopause: coordinated four-point magnetic field measurements, *Ann. Geophys.*, *19*, 1449.

Dunlop, M. W., A. Balogh, and K. H. Glassmeier (2002), Four-point Cluster application of magnetic field analysis tools: The discontinuity analyzer, *J. Geophys. Res.*, *107*(A11), 1385, doi:10.1029/2001JA005089.

Fairfield, D. H. (1971), Average and unusual locations of the Earth's magnetopause and bow shock, *J. Geophys. Res.*, *76*, 6700.

Futaana, Y., et al. (2006a), First ENA observations at Mars: Subsolar ENA jet, *Icarus*, *182*, 413.

Futaana, Y., S. Barabash, A. Grigoriev, D. Winningham, R. Frahm, M. Yamauchi, and R. Lundin (2006b), Global response of Martian plasma environment to an interplanetary structure: From ENA and plasma observations at Mars, *Space Sci. Rev.*, *126*, 315.

Grigoriev, A., Y. Futaana, S. Barabash, and A. Fedorov (2006), Observations of the Martian Subsolar ENA Jet Oscillations, *Space Sci. Rev.*, *126*, 299.

Halland, S. E., et al. (2004), Four-spacecraft determination of magnetopause orientation, motion and thickness: comparison with results from single-spacecraft methods, *Ann. Geophys.*, *22*, 1347.

Holmstrom, M., S. Barabash, and E. Kallio (2002), Energetic neutral atoms at Mars: 1. Imaging of solar wind protons, *J. Geophys. Res.*, *107*(A10), 1277, doi:10.1029/2001JA000325.

Iyemori, T., and D. R. K. Rao (1996), Decay of the Dst component of geomagnetic disturbance after substorm onset and its implication to storm substorm relation, *Ann. Geophys.*, *14*, 608.

McComas, D. J., R. C. Elphic, M. B. Moldwin, and M. F. Thomsen (1994), Plasma observations of magnetopause crossings at geosynchronous orbit, *J. Geophys. Res.*, *99*, 21,249.

Milan, S. E., S. W. H. Cowley, M. Lester, D. M. Wright, J. A. Slavin, M. Fillingim, C. W. Carlson, and H. J. Singer (2004), Response of the

magnetotail to changes in the open flux content of the magnetosphere, *J. Geophys. Res.*, *109*, A04220, doi:10.1029/2003JA010350.

Moore, T. E., et al. (2000), The low energy neutral atom imager for IMAGE, *Space Sci. Rev.*, *91*, 155.

Moore, T. E., et al. (2001), Low energy neutral atoms in the magnetosphere, *Geophys. Res. Lett.*, *28*, 1143.

Moore, T. E., M. R. Collier, M.-C. Fok, S. A. Fuselier, H. Khan, W. Lennartsson, D. G. Simpson, G. R. Wilson, and M. O. Chandler (2003), Heliosphere-geosphere interactions using low energy neutral atom imaging, *Space Sci Rev.*, *109*, 351.

Murata, Y., S. Taguchi, K. Hosokawa, A. Nakao, M. R. Collier, T. E. Moore, N. Sato, H. Yamagishi, and A. S. Yukimatu (2007), Correlative variations of the neutral atom emission in the high-altitude cusp and the fast anti-sunward convection in the low-altitude cusp, *J. Geophys. Res.*, *112*, A11208, doi:10.1029/2007JA012404.

Ober, D. M., M. F. Thomsen, and N. C. Maynard (2002), Observations of bow shock and magnetopause crossings from geosynchronous orbit on 31 March 2001, *J. Geophys. Res.*, *107*(A8), 1206, doi:10.1029/2001JA000284.

Petrinec, S. M., and C. T. Russell (1996), Near-Earth magnetotail shape and size as determined from the magnetopause flaring angle, *J. Geophys. Res.*, *101*, 137.

Rairden, R., L. Frank, and J. Craven (1986), Geocoronal imaging with Dynamics Explorer, *J. Geophys. Res.*, *91*(A12), 13,613.

Roelof, E. C., and D. G. Sibeck (1993), Magnetopause shape as a bivariate function of interplanetary magnetic field B_z and solar wind dynamic pressure, *J. Geophys. Res.*, *98*, 21,421.

Shield, M. A. (1969), Pressure balance between solar wind and magnetosphere, *J. Geophys. Res.*, *74*, 1275.

Shue, J.-H., J. K. Chao, H. C. Fu, C. T. Russell, P. Song, K. K. Khurana, and H. J. Singer (1997), A new functional form to study the solar wind control of the magnetopause size and shape, *J. Geophys. Res.*, *102*, 9497.

Shue, J.-H., et al. (1998), Magnetopause location under extreme solar wind conditions, *J. Geophys. Res.*, *103*, 17,691.

Sibeck, D. G., R. E. Lopez, and E. C. Roelof (1991), Solar wind control of the magnetopause shape, location, and motion, *J. Geophys. Res.*, *96*, 5489.

Taguchi, S., M. R. Collier, T. E. Moore, M.-C. Fok, and H. J. Singer (2004), Response of neutral atom emissions in the low- and high-latitude magnetosheath direction to the magnetopause motion under extreme solar wind conditions, *J. Geophys. Res.*, *109*, A04208, doi:10.1029/2003JA010147.

Taguchi, S., S.-H. Chen, M. R. Collier, T. E. Moore, M.-C. Fok, K. Hosokawa, and A. Nakaso (2005), Monitoring the high-altitude cusp with the Low Energy Neutral Atom imager: Simultaneous observations from IMAGE and Polar, *J. Geophys. Res.*, *110*, A12204, doi:10.1029/2005JA011075.

Taguchi, S., K. Hosokawa, A. Nakao, M. R. Collier, T. E. Moore, A. Yamazaki, N. Sato, and A. S. Yukimatu (2006), Neutral atom emission in the direction of the high-latitude magnetopause for northward IMF: Simultaneous observations from IMAGE spacecraft and SuperDARN radar, *Geophys. Res. Lett.*, *33*, L03101, doi:10.1029/2005GL025020.

M. R. Collier and T. E. Moore, NASA Goddard Space Flight Center, Greenbelt, MD 20771, USA. (michael.r.collier@nasa.gov; tmoore@pop600.gsfc.nasa.gov)

K. Hosokawa, S. Suzuki, and S. Taguchi, Department of Information and Communication Engineering, University of Electro-Communications, 1-5-1 Chofugaoka, Chofu, Tokyo 182-8585, Japan. (hosokawa@ice.uec.ac.jp; shin.s@ice.uec.ac.jp; taguchi@ice.uec.ac.jp)

M. F. Thomsen, Los Alamos National Laboratory, Los Alamos, NM 87545, USA. (mthomsen@lanl.gov)